J. Fluid Mech. (1990), *vol.* 210, *pp.* 415–435
Printed in Great Britain

Frequency of sublayer bursting in a curved bend

By MOHAMMED ANWER AND RONALD M. C. SO
Mechanical and Aerospace Engineering, Arizona State University, Tempe, AZ 85287-6106, USA

(Received 15 December 1987 and in revised form 3 July 1989)

The characteristics of sublayer bursting in turbulent pipe flow through a 180° curved bend at a pipe Reynolds number of 50000 were investigated. In particular, the effects of bend curvature on the bursting frequency were studied in detail. A flush-mounted shear stress gauge was used to measure the wall shear stress and the VITA technique was applied to isolate the bursting events in the wall shear signals. The results show that the bursting frequency starts to drop rather dramatically at the inlet region of the inner bend (closest to the centre of curvature of the bend). Contrary to expectation, the bursting frequency remains fairly constant along the outer bend, but increases sharply as the flow comes out of the bend. Possible explanations for this behaviour are proposed based on the important external effects present in a pipe bend; that is, those due to centrifugal force, streamline curvature and the superimposed secondary flow. Even though wall pressure measurements show that the flow recovers to a fully developed straight pipe condition at a short distance downstream of the bend exit, the circumferential wall shear stress distribution, the spectral content of the wall shear signal and the associated bursting frequency suggest that the near-wall flow takes a much longer distance to return to an unperturbed straight-pipe condition.

1. Introduction

The characteristics of sublayer flow were investigated by F. R. Hama in an unpublished work. In that study, the near-wall turbulent boundary-layer flow was investigated using dye injection through a slot in the wall. Downstream of the slots, the dye was observed to coagulate into longitudinal streaks. Similar features were also observed by Hama in an artificially perturbed laminar boundary layer. These results were quoted by Corrsin (1957) in his report on current problems of turbulent shear flows. Later, in a more detailed study, Kline, Reynolds & Schraub (1967) examined the generation of these streaks as a function of the normal distance from the wall. They found that regions of slower moving and faster moving fluids coexisted side-by-side in the sublayer, and an intermittent period of 'bursting' was observed. Low-speed streaks would lift from the surface and develop into vortices either in the transverse or in the longitudinal direction. Finally, these vortices would lift up from the sublayer and would be convected towards the core region of the flow.

Corino & Brodkey (1969) studied, in considerable detail, the behaviour of the near-wall region of a fully developed turbulent pipe flow. High-speed motion pictures of a very small region of the flow near the wall were taken using a camera that was kept stationary with respect to the mean flow. Similar to the boundary-layer observation of Kline *et al.* (1967), an intermittent period of 'bursting' was observed in which fluid would eject from the sublayer and would be carried into the core region of the flow. These events were found to be distributed randomly in space and time. This similar

behaviour observed between the bursting process in a pipe flow and a boundary-layer flow is consistent with the similarities found between the measured characteristics of near-wall flow in a pipe (Laufer 1954) and in a flat-plate boundary-layer (Klebanoff 1955). Therefore, the burst finding further substantiates the general nature of the near-wall flow.

Most of these violent ejections take place in the region $y^+ < 15$ and have an axial dimension of 20–40 viscous lengths, where $y^+ = yw_\tau/\nu$, y (mm) being the normal coordinate measured from the wall, w_τ (cm/s) the friction velocity and ν (m^2/s) the fluid kinematic viscosity. Lu & Willmarth (1973) observed that there is a violent fluctuation of Reynolds stress at the wall associated with the bursting event, while Falco (1978) found that 70% of the net turbulence production is associated with the bursting events. Since these early studies, a lot has been learnt about the behaviour of sublayer bursting both in internal flows and in boundary-layer flows. Based on these earlier results and visual observation of the generation of turbulent spots in a boundary layer, Perry, Lim & Teh (1981) explained the bursting behaviour using the ideas of counter-rotating vortices originally proposed by Theodorsen (1952, 1955). The existence of these counter-rotating vortices within the sublayer has been demonstrated by several techniques. Bakewell & Lumley (1967) demonstrated their existence by eigenfunction decomposition of space–time correlation of streamwise fluctuating velocity. On the other hand, Smith (1978) and Head & Bandyopadhyay (1981) investigated such vortices visually, while Head & Bandyopadhyay (1978) and Blackwelder (1978) carried out measurements within them. Recently, Moin & Kim (1985) and Kim & Moin (1986) calculated these vortices numerically in a turbulent channel flow using large-eddy simulation technique. A mathematical model has also been attempted by Perry & Chong (1982).

While the exact reasons for the formation of these vortices are not known, several theories have been proposed. Some researchers (e.g. Moin & Kim 1985) believe that they are generated by the deformation of the mean vortex sheet by turbulence, while others (e.g. Coles 1978; Brown & Thomas 1977) suggest that Taylor–Görtler-type instabilities within the sublayer are responsible for their formation. Another explanation for sublayer bursting which discards the counter-rotating vortices theory was proposed by Kobashi & Ichijo (1986) who suggested that local adverse pressure set up within the sublayer by turbulence is responsible for the formation of counter-rotating vortex rings rather than counter-rotating vortices. These counter-rotating vortex rings are responsible for sublayer bursting.

Whatever the reason for sublayer bursting, it is an important feature of wall-bounded shear flows. Therefore, its study could shed further light on the understanding of both complex and simple turbulent shear flows. Furthermore, it is important to understand how external effects could influence bursting and hence the characteristics of the near-wall flow. While a considerable amount of information is available on the behaviour of sublayer bursting in both boundary-layer and internal flows, almost nothing is known about the influence of external effects on bursting (Kline 1978). The investigation of sublayer bursting in complex flows with external effects could enhance our understanding of the bursting process as well as the characteristics of complex turbulent wall shear flows.

An experimental investigation was carried out to investigate the bursting phenomenon in a curved bend and its subsequent relaxation in a downstream straight pipe. Some of the features present in a curved pipe flow are unique and could have significant influence on the bursting phenomenon. These features include: (i) a completely three-dimensional flow, (ii) a destabilizing effect along the outer bend

which is concave and a stabilizing effect along the inner bend which is convex, (iii) a superimposed secondary motion which produces a jet impingement phenomenon on the outer bend and a boundary-layer merging phenomenon on the inner bend, (iv) a Dean-type secondary motion which gives rise to a flow over a concave surface along the circumference of the pipe, and (v) an abrupt disappearance of the centrifugal force as the flow exits from the bend, and this in turn, causes a sudden deceleration of the secondary motion. Some of these features could significantly affect the large structures in the flow and hence perturb the behaviour of sublayer bursting. Furthermore, So & Mellor (1975) found evidence of Taylor–Görtler-type vortices superimposed on the turbulent boundary-layer flow over a concave surface. They arrived at their conclusion based on static pressure measurements across the boundary layer. More recently, Moser & Moin (1987) used a direct simulation technique to calculate a turbulent boundary layer on a concave surface and found evidence of stationary Taylor–Görtler-type vortices. These vortices were found to have significant effect on the flow because they contribute to the mean Reynolds stress field. In view of these findings, bend curvature is expected to have significant effects on sublayer bursting.

A study was undertaken to investigate the influence of all these external effects on a fully developed turbulent flow through a 180° curved bend and its subsequent relaxation downstream of the bend. The flow characteristics as well as the bursting behaviour were studied in detail. This paper reports on the sublayer bursting phenomenon, while the measured flow behaviour is reported separately (Anwer, So & Lai 1989).

2. Experimental set-up and instrumentation

The experimental rig consisted of two straight Plexiglas pipes connected by a 180° bend. Care was taken to ensure that all the joints were smooth and that there were no steps present anywhere in the test rig. The straight sections have a diameter of 7.6 cm and were approximately 7.6 m, or 100 diameters long. This length was sufficient to ensure a fully developed flow upstream of the entrance to the bend and at the exit of the rig. Air flow through the rig was provided by a centrifugal blower installed at the exit. A small air gap was provided between the blower and the rig to prevent blower vibration from transmitting through the rig. At the entrance to the pipe, a bell-shaped inlet and a honeycomb flow straightener were installed. The bend used in the present experiments had an α-value of 0.077, where $\alpha = a/R$, a being the radius of the pipe and R the mean radius of the bend. The 180° bend was formed by connecting two 90° bends which were formed by bending straight sections of Plexiglas pipe. This produced a pipe bend with cross-sectional area not quite circular at some section of the bend. The maximum variation of the cross-sectional diameter was 1 mm. This small variation in diameter was found to have little or no effect on the general behaviour of the flow in the bend (Anwer *et al.* 1989). The establishment of a fully developed turbulent flow upstream of the bend at a Reynolds number $Re = W_0 D/\nu = 50000$ (where W_0 is the mean bulk velocity in m/s) was verified by measuring the wall static pressure drop along the pipe. This was accomplished by installing wall pressure taps along one pipe generator in the upstream straight pipe. However, starting at a distance of 18 diameters upstream of the bend, pressure taps were placed at regular intervals on two diametrically opposite generators and continued to a distance of 18 diameters downstream of the bend. Therefore, the pressure on opposite sides of the curved bend could be measured in detail. The

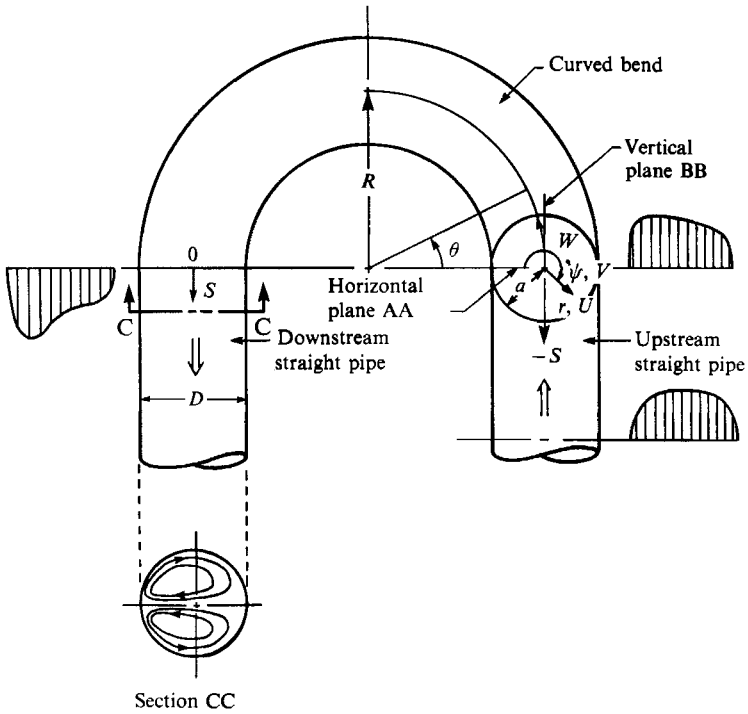

FIGURE 1. Schematic of flow through a pipe bend and definition of axes.

pressure taps were circular holes with sharp edges and were 1.5 mm in diameter. Tygon tubing was used to connect the pressure taps to a variable capacitance pressure transducer (Rosemount Engineering Model 831A4) via a 48 channel scanivalve. A pressure tap at 26 diameters upstream of the curved bend was selected as the reference pressure for the wall pressure drop measurements in the region bounded by $S/D = -18$ to 18, where S is the axial distance and measures zero at both bend entrance and exit and D is the pipe diameter (figure 1).

Dean-type secondary motions are set up in the curved bend owing to an imbalance between the radial pressure gradient and the centrifugal force. These secondary motions persist for quite some distance in the downstream straight pipe (Azzola *et al.* 1986; Anwer *et al.* 1989). As a result, wall shear stress cannot be deduced from static pressure measurements alone. Besides, the wall shear distribution around the circumference of the pipe is not uniform. Therefore, it is necessary to measure the wall shear distribution in both the straight and curved sections of the pipe bend test rig.

A DISA 55R45 flush-mounted hot-film probe was used together with a DISA 56C01 constant-temperature anemometer and a DISA 56C16 general purpose bridge to measure wall shear stress. The shear stress gauge was calibrated in the fully developed turbulent pipe flow upstream of the bend. In this region of the flow the pressure drop ($\Delta P/\Delta S$) and the mean wall shear (τ_w) are related by $\tau_w = \frac{1}{2}a(\Delta P/\Delta S)$. Because of the small variation of the mean bridge voltage (e) with mean shear, the signal was not linearized for processing. Instead, an expression like

$$e^2 = e_0^2 + B\tau_w^n,$$

where e_0 is the bridge voltage at zero flow and B and n are constants, was used to

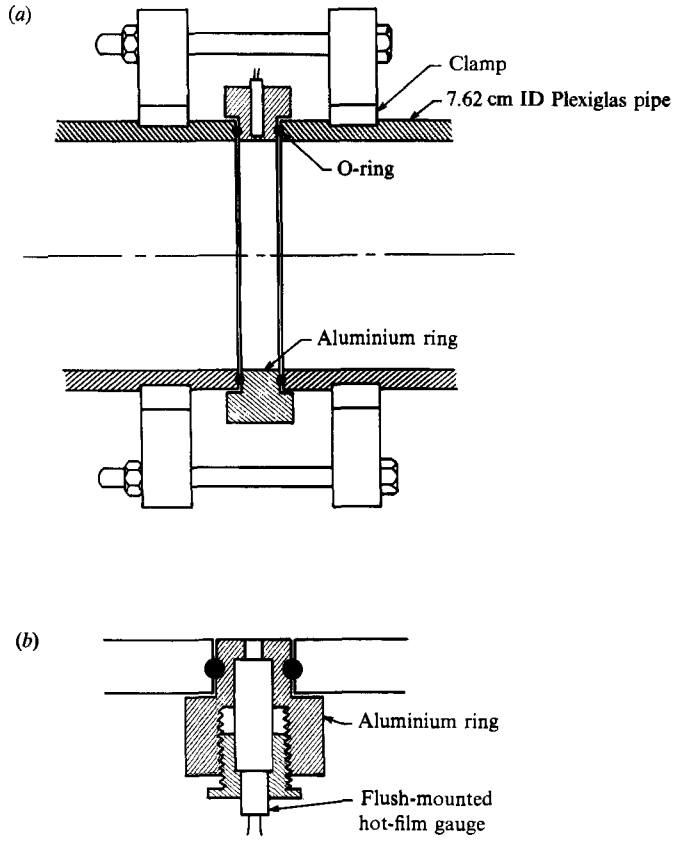

FIGURE 2. Assembly of the pipe ring used for wall shear stress measurements. (*a*) Set-up for shear stress measurement, (*b*) close-up of the shear stress gauge.

approximate τ_w (N/m^2) and was found to give mean shear stress accurate to within 0.5%. The exponent was found to vary from 0.32 to 0.38. This method of measuring wall shear stress is very reliable and has been validated and used by such researchers as Menendez & Ramaprian (1985), Mautner & Van Atta (1986). Furthermore, the wall shear stress signal can be processed to give information about the bursting phenomenon (Strickland & Simpson 1975).

The hot-film sensor is 0.2 mm wide and 0.75 mm in length. Therefore, the sensing element corresponds to 15 viscous lengths, which is well within the limit proposed by Ligrani & Bradshaw (1987) for accurate measurements of the properties of small-scale turbulence in the near-wall region. Furthermore, heat transfer from a sensor placed in the substrate, like the hot-film probe used in this study, is different from the heat transfer from a hot-wire sensor placed in the flow. Consequently, the frequency response of a wall-mounted sensor could be significantly different from that of a hot wire (Bellhouse & Schultz 1966). The frequency response of the wall-mounted sensor used in this study was estimated to be of the order of 100 kHz. This is almost two orders of magnitude higher than the dynamic range of the flow estimated from the Kolmogorov timescale.

The surface hot-film probe was mounted on an aluminium ring (figure 2*a*) that could be moved to any desired axial location of the test rig. A detailed drawing showing the mounting of the shear stress gauge in the ring is shown in figure 2 (*b*). The

pipe was cut at the desired axial location, and the ring was secured to the pipe by two clamps (figure 2*a*) which allowed the ring to be rotated around the pipe. Extreme care was taken to match the inner surfaces of the pipes and the ring, so that no step resulted from the arrangement. A small portion of the bend was shaved off to compensate for the thickness of the ring. Within the bend, the placing of the ring corresponded to a 6 mm straight section in a bend of radius 49 cm. Leakage was prevented by installing O-rings between the aluminium ring and the Plexiglas pipe. Therefore, this set-up permitted the wall shear distribution around the circumference to be measured using only one shear stress gauge. Since the flow is symmetric about the horizontal plane in both straight and curved sections, wall shear measurements were carried out around the top half of the bend only.

All data were collected using a 12 bit resolution Metrabyte DAS-16 A/D converter together with a desk top personal computer. Although the bursting frequency is comparatively low, the bursting event itself takes place over a very short interval of time. Therefore, it is necessary to obtain as many samples as possible in this short interval of time. The raw data were recorded at a sampling rate of 20 kHz. However, the data record was limited to one second because of the memory buffer limitation of the A/D converter. Three data records were collected and analysed separately. All the data were later transferred to an IBM3090 mainframe for detailed analyses using vector operations.

The coordinate system used in the present study is shown in figure 1. Shear stress measurements were obtained at ten locations along the pipe: $S/D = -18, -1$, $\theta = 22.5°$, $67.5°$, $112.5°$, $157.5°$, $S/D = 1$, 6, 10 and 18, where θ is the angular measure along the bend. The analyses of the bursting phenomenon were carried out at $\psi = 0°$ (inner bend), $\psi = 90°$ (top of the bend) and $\psi = 180°$ (outer bend), where ψ is the angular measure around the circumference of the pipe.

3. Detection technique

A major problem in the experimental investigation of sublayer bursting is the detection of a burst in the raw signal. Most of the information available on sublayer bursting is descriptive in nature and obtained from flow visualization experiments. Often, it is difficult to 'translate' this qualitative information into an algebraic description. The success of a detection algorithm depends mainly on how effectively the algorithm can simulate the actual condition observed in the flow visualization studies. In the present study, the variable interval time averaging (VITA) technique was used to detect bursts. As an independent check, the autocorrelation technique was also used to obtain the bursting frequency in the straight pipe.

Details of the VITA technique are given elsewhere (Blackwelder & Kaplan 1976; Johansson & Alfredsson 1982), but a brief review is provided here for convenience. Variable interval time averaging of a signal $u(x_i, s)$ at location x_i, and fluctuating in time coordinate s is defined as

$$\hat{u}(x_i, t; T) = \frac{1}{T} \int_{t-\frac{1}{2}T}^{t+\frac{1}{2}T} u(x_i, s)\, \mathrm{d}s,$$

where T is the averaging time. As T becomes large, conventional averaging is achieved, that is,

$$\bar{u}(x_i) = \lim_{T \to \infty} \hat{u}(x_i, t; T).$$

An unbiased estimate of the mean can be obtained only if the integration time T is

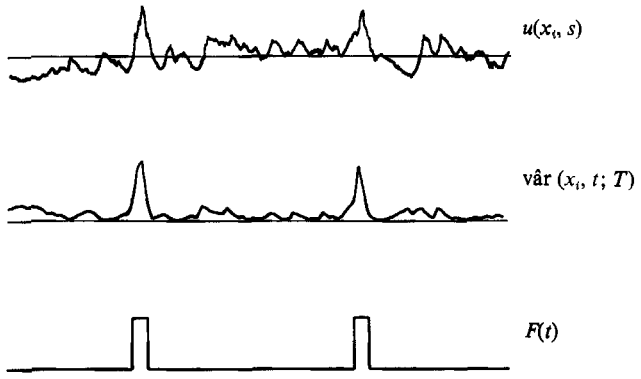

FIGURE 3. Effect of passing a signal through the VITA algorithm.

greater than the stationary period of the signal. In order to obtain an estimate of the local turbulent kinetic energy, a localized variance is defined, such that

$$\hat{\text{var}}\,(x_i, t; T) = \hat{u}^2(x_i, t; T) - [\hat{u}(x_i, t; T)]^2.$$

Algebraically, $\hat{\text{var}}\,(x_i, t; T)$ should be a positive definite quantity. The detection function $F(t)$ is defined as

$$F(t) = 1 \quad \text{if } \hat{\text{var}}\,(x_i, t; T) > k u_{\text{rms}}^2 \quad \text{and} \quad \partial u/\partial t > 0,$$

or

$$F(t) = 0 \quad \text{otherwise.}$$

where k is a threshold value, and u_{rms}^2 is the unbiased variance of the signal. A burst is detected if $F(t) = 1$. Figure 3 shows the effect of allowing a signal to pass through the VITA algorithm.

For bursting analysis, VITA was originally developed using near-wall velocity fluctuation signals. In this study, VITA is used to analyse wall shear stress fluctuation signals. This is because the near-wall flow in a curved bend is highly three-dimensional; therefore, it is not at all clear what combination of components of velocities the sensor will measure in such a flow. Strickland & Simpson (1975) have successfully used the autocorrelation technique to analyse shear stress fluctuation signals to detect bursts. On the other hand, Lu & Willmarth (1973) have observed a violent fluctuation of Reynolds stress associated with the bursting event and Brown & Thomas (1977) have demonstrated by simultaneous wall shear stress and near-wall velocity measurements that, near the wall, the fluctuation of velocity is very similar to the fluctuation of wall shear stress. Since the fluctuations of near-wall velocity and wall shear stress are similar, and the VITA technique essentially isolates the events of high fluctuation in the signal, it should be equally applicable to the signals of wall shear stress fluctuation.

The VITA algorithm is essentially a mathematical low-pass filter. Therefore, burst detection is a strong function of the integration time T and the threshold level k. A threshold value of 1.2 and a non-dimensional integration time of $Tw_\tau^2/\nu = 17$ were used in this investigation. These values compare well with a threshold value of 1.2 and a non-dimensional integration time of $Tw_\tau^2/\nu = 10$ used by Blackwelder & Kaplan (1976). The integration time and threshold value were chosen to match the bursting results obtained from flow visualization experiments in straight pipes. However, it should be mentioned here that the absolute magnitudes of these values are not of importance, because the objective of this study is to evaluate the relative

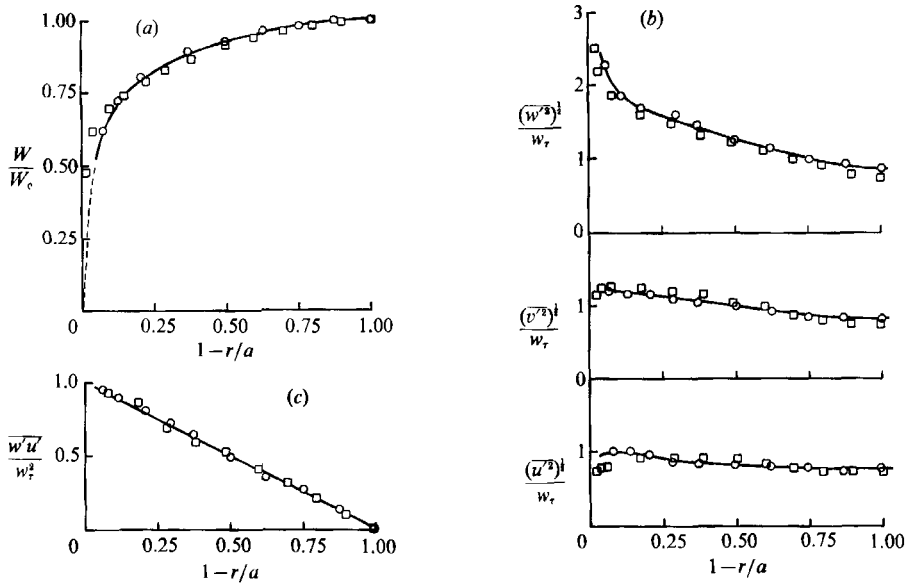

FIGURE 4. Comparison of measurements at $S/D = -18.0$ in the upstream straight pipe to those of Laufer (1954): —○— present measurement; —□— measurements of Laufer. (*a*) Axial velocity, (*b*) normal stresses, $(\overline{w'^2})^{\frac{1}{2}}/w_\tau$, $(\overline{v'^2})^{\frac{1}{2}}/w_\tau$, and $(\overline{u'^2})^{\frac{1}{2}}/w_\tau$, (*c*) shear stress $\overline{w'u'}/w_\tau^2$.

effects of bend curvature on sublayer bursting rather than absolute behaviour. Therefore, once these values were chosen, they were kept constant throughout the study.

Besides the VITA technique, the autocorrelation technique was also used for burst detection in the straight pipe. For comparison, both techniques were used to determine the bursting frequency at $S/D = -18$. Mean flow velocity and turbulence measurements were also carried out at $S/D = -26$ and -18 using a modified rotating-wire technique (Anwer *et al.* 1989), and were checked for their fully developed characteristics by comparing to the measurements of Laufer (1954) at $Re = 50000$, see figure 4. The measurements at $S/D = -26$ and -18 are essentially identical; therefore, only those at $S/D = -18$ are shown in figure 4 for comparison with Laufer's measurements. These comparisons indicate that the flow at $S/D = -26$ and -18 is indeed fully developed. Hence, the bursting frequency measurements at these locations could be compared with other literature data. An extensive review of the results of bursting frequency measurements in pipe and boundary-layer flows had been carried out by Bogard & Tiederman (1986). A summary comparison of these results with the present measurements obtained at $S/D = -18$ is given in table 1. From this comparison, it can be seen that the present measurements, deduced from both the VITA and autocorrelation techniques are in good agreement with those reported in the literature.

A sample autocorrelation of the wall shear stress $R_{11}(\tau)$, where τ is the time delay, obtained at $S/D = -18$ is shown in figure 5. The overall behaviour of the autocorrelation is similar to the earlier results of Strickland & Simpson (1975) and of Heidrick, Banerjee & Azad (1977). Strickland & Simpson (1975) and Kim, Kline & Reynolds (1971) had also attempted to determine the bursting frequency in a boundary-layer flow by examining the autocorrelation of a 'short'-period time series signal. The average interburst time was taken to be the time delay corresponding to

Work	Flow	Detection technique	Re_θ	$T_B W_c/\delta$
Ueda & Mizushima (1979)	pipe	(u, v)-quadrant truncation	200	5.1
Sabot & Comte-Bellot (1976)	pipe	(u, v)-quadrant truncation	4800	4.7
Heidrick *et al.* (1977)	pipe	Spatial derivative	1120	3.2
Achia & Thompson (1977)	pipe	Flow visualization	580	4.7
Strickland & Simpson (1975)	boundary layer	Autocorrelation	2000	5.2
Kim *et al.* (1971)	boundary layer	Autocorrelation	600	6.2
Present	pipe	VITA	2400	5.4
Present	pipe	Autocorrelation	2400	5.7

TABLE 1. Comparison of burst frequency measurements in fully developed pipe and boundary-layer flows. Here, Re_θ is Reynolds number based on momentum thickness θ, T_B denotes the average time between bursts, W_c the centreline velocity for a fully developed pipe flow, or free-stream velocity for a boundary-layer flow, and δ the radius of the pipe for a fully developed pipe flow, or the boundary-layer thickness for a boundary-layer flow.

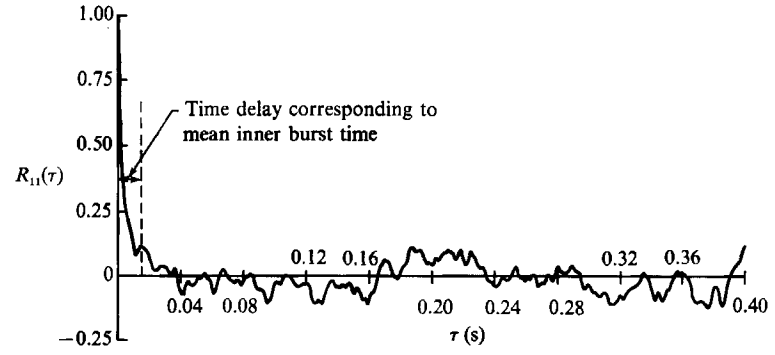

FIGURE 5. Autocorrelation of wall shear stress signal measured in the straight pipe.

the first peak in the autocorrelation. For this case, a 'short' period is considered to be a sample length shorter than two orders of magnitude greater than the mean interburst time. A longer sample length would not show any 'discernible peaks' (Strickland & Simpson 1975) in the autocorrelation. According to this definition, all the samples of the present study corresponded to 'short'-period signals. However, no 'discernible peaks' were observed in the autocorrelation of any of the samples recorded in the straight pipe. On the other hand, when a much shorter sample (of the order of 10 bursting period) was analysed, one or more peaks were observed at time delay corresponding to the mean interburst time. Within the bend section, especially along the top of the bend, even such a 'short' sample failed to give any peak corresponding to the bursting period. In most cases, a small 'kink' was observed in the autocorrelation and peaks could be obtained only by further shortening the sample length under consideration for the autocorrelation. Hence no fixed sample length could be determined for the autocorrelation technique. From this investigation, it is evident that the autocorrelation technique is relatively more subjective than the VITA technique. Therefore, in the subsequent investigation all analyses were carried out using the VITA technique.

4. Results and discussion

The primary objective of this study was to examine the relative effects of bend curvature on the bursting phenomenon. Near-wall measurements of the velocity and turbulence fields were not used to determine the bursting frequency. This is primarily because of the complexity involved in carrying out measurements in the geometry of a curved bend. The flow inside a curved bend is three-dimensional. Therefore, simple diagnostic techniques, such as single and $\times$-wires, are not appropriate for this flow. Furthermore, it is difficult to resolve the three-dimensional near-wall flow using a multi-wire sensor without substantially disturbing the flow and severely compromising the spatial resolution of the measurements. On the other hand, there are other problems associated with the use of a laser Doppler velocimeter (LDV) to measure such a flow. A three-component LDV could be used to resolve the flow; however, pipe curvature poses a different problem for the experiments (Durrett, Stevenson & Thompson 1985). Since Strickland & Simpson (1975) have established the use of wall shear stress for burst detection in a boundary layer, the same technique was adopted for this investigation. Besides wall shear, other measurements were also carried out to characterize the near-wall flow behaviour in the bend. These were wall static pressure measurements along the inner and outer bends and the wall shear stress distributions around the circumference of the pipe.

4.1. *Static pressure and mean shear*

As a fully developed pipe flow enters a pipe bend, the curvature of the streamlines creates a radial pressure gradient towards the centre of the curvature of the bend. Owing to the elliptic nature of incompressible viscous flow, this pressure gradient propagates upstream into the straight pipe through the wall boundary layers. Consequently, the distributions of the wall static pressure, expressed as $(p-p_0)/\frac{1}{2}\rho W_0^2$, where ρ is the fluid density, p is the wall static pressure and p_0 is the wall static pressure at $S/D = -26$, along $\psi = 0°$ and $\psi = 180°$ start to deviate from each other even before the flow enters the bend (figure 6). Within the bend, the imbalance between the centrifugal force and the radial pressure gradient sets up two Dean-type secondary flow cells. The magnitude of this secondary flow depends greatly on the bend curvature, which, in turn, also determines the pressure difference between the outer and the inner bend. A maximum pressure difference is noted at $\theta \approx 112°$ (figure 6). When the flow emerges from the bend, it relaxes, and eventually returns to the fully developed straight pipe condition. Present results indicate that the effects of bend curvature are felt at $S/D \approx -5$ and that they disappear at about the same distance downstream of the bend; that is, starting at $S/D = 5.0$ the pressure drop is again linear and closely parallels the axial pressure drop curve in the upstream straight pipe. This seems to indicate that a fully developed pipe flow condition is again achieved at $S/D = 5.0$.

The distribution of mean shear τ_w (where $\tilde{\tau}_w = \tau_w + \tau'_w$, $\tilde{\tau}_w$ being the instantaneous wall shear and τ'_w the fluctuating part of $\tilde{\tau}_w$) along the bend follows closely that of the wall static pressure. Just as in the case of the wall static pressure, it is observed that the mean shear, plotted in terms of the skin-friction coefficient $C_f = 2\tau_w/\rho W_0^2$, decreases on the inner bend (figure 7*a*) and increases on the outer bend (figure 7*b*) as the flow enters the bend. In spite of this similarity, some irregularities are noticed in the τ_w distribution along the inner bend. First, τ_w increases slightly at $S/D = -1$ before decreasing drastically at the entrance to the bend (figure 7*a*). Secondly, an increase is observed around $\theta = 90°$. This is again followed by a drastic decrease at

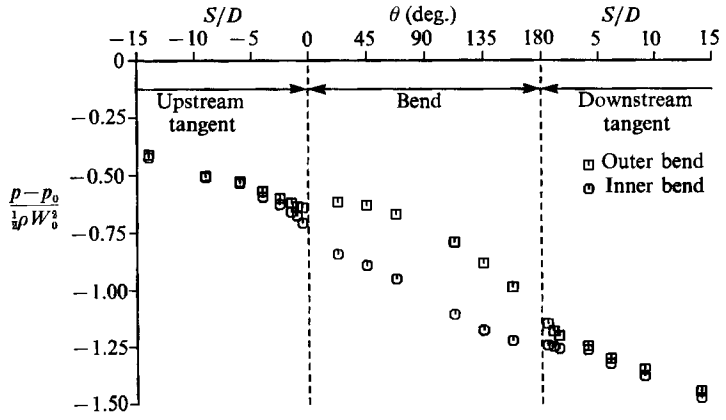

FIGURE 6. Wall static pressure measurements along the curved bend.

$\theta = 110°$. The decrease of wall shear continues up to $S/D = 1.0$ in the downstream straight pipe. Beyond this location the wall shear begins to recover. However, the τ_w values on both the inner and outer bends do not recover to their unperturbed straight pipe value even at $S/D = 18$. The reasons for these irregularities are not known. However, it is clear that the irregularities are not caused by errors in the measurement of τ_w.

A large increase in mean shear is also observed in the bend section at the top of the bend (figure 7*c*). However, the increase is not as large as that measured in the outer bend (figure 7*b*). This increase could be attributed to the cross-flow set up around the pipe by the secondary motion and to the fact that the cross-flow is over a concave surface. The wall shear recovery is faster than that on the outer bend. Unlike the wall shear on the inner and outer bends, the wall shear on the top of the bend recovers to its undisturbed value at $S/D = 18$.

The circumferential distributions of C_f at various stream locations are shown in figure 8. At $S/D = -18$ the C_f distribution around the pipe is quite uniform, while at $S/D = -1$ the variation of C_f around the pipe is rather prominent (figure 8). This seems to substantiate the fact that the upstream influence of bend curvature is limited to $S/D > -18$. In general, the C_f variation around the pipe circumference increases continuously until $\theta = 112.5°$. Thereafter, it begins to decrease. These trends are in agreement with the measured pressure difference between the inner and outer bends at different θ, except for the approach to a fully developed straight pipe condition. While the pressure drop measurements indicate that the fully developed straight pipe condition is again achieved at $S/D = 5$, the C_f measurements at $S/D = 10$ still show substantial variation around the pipe. Even at $S/D = 18$, the C_f variation is small but noticeable. This means that a truly fully developed straight pipe condition still has not been reached at $S/D = 18$.

4.2. *Bursting frequency and higher moments*

The bursting frequency results, expressed as af_b/W_0, where f_b is the burst frequency, are shown in figure 9. Overall, there is a tremendous perturbation of the bursting phenomenon due to bend curvature. Along the inner bend, the bursting frequency starts to increase at $S/D = -1$. However, as the flow enters the bend, the bursting frequency starts to drop dramatically on the inner bend and then recovers gradually as the flow exits the bend. The increase in bursting frequency before the bend

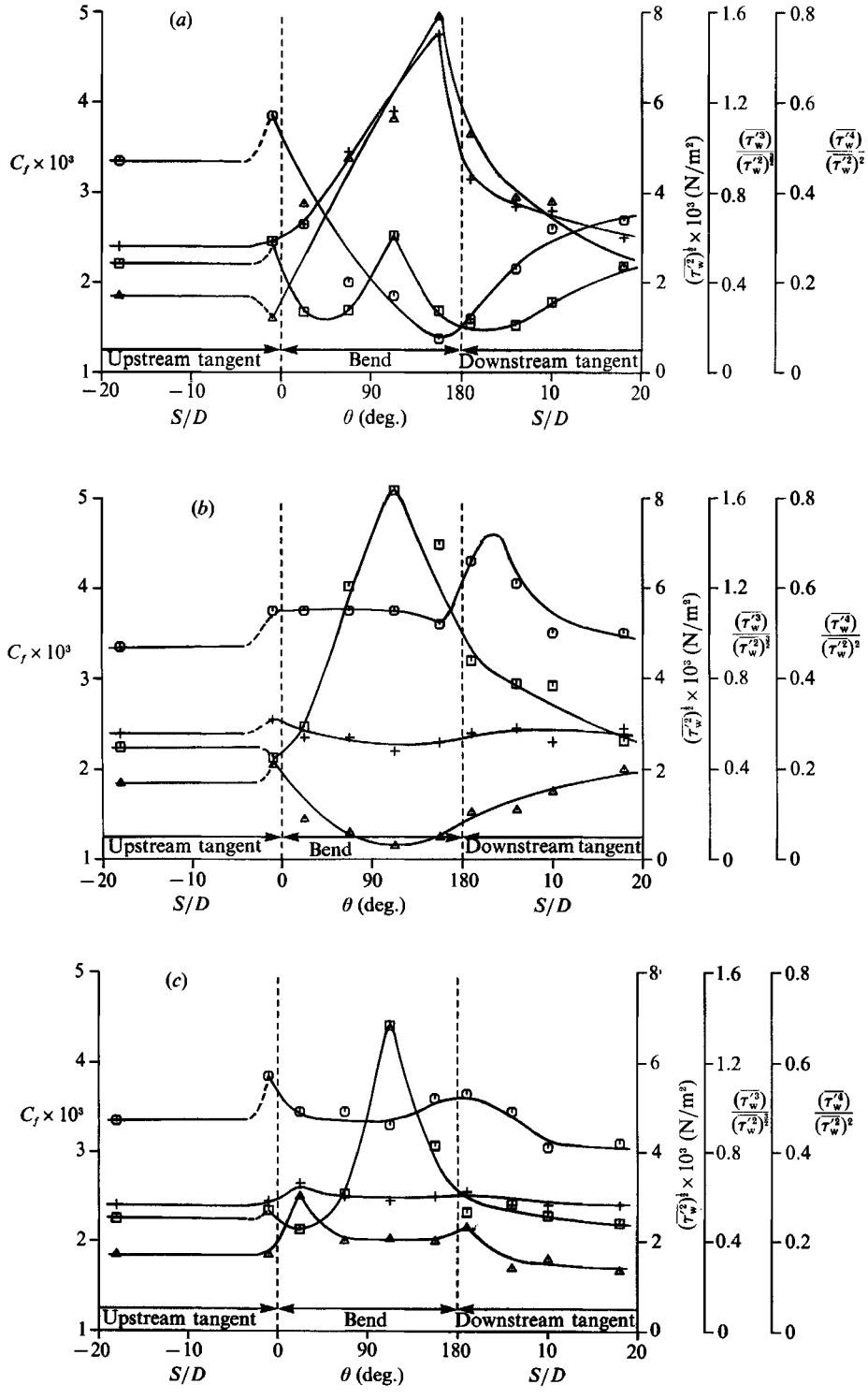

FIGURE 7. First four moments of wall shear stress signals: —□— mean, —⊙— standard deviation, —△— skewness, —+— kurtosis. (*a*) Inner bend, (*b*) outer bend, (*c*) top of the bend.

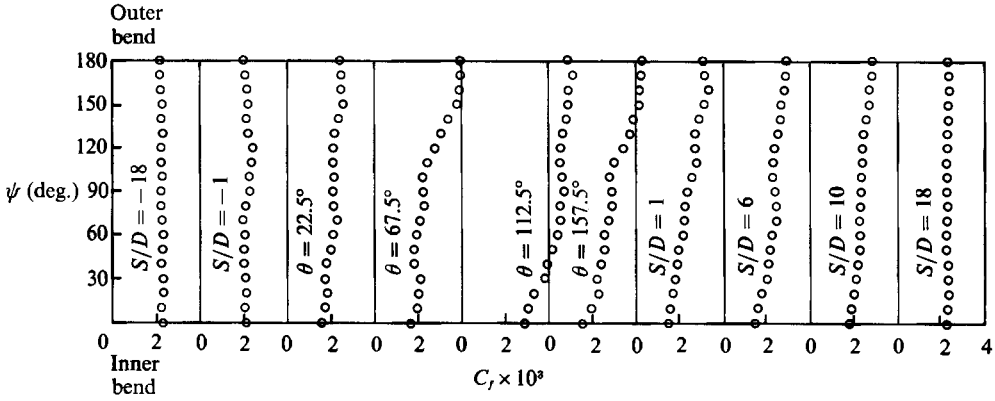

FIGURE 8. Evolution of the mean shear stress distribution along the curved bend.

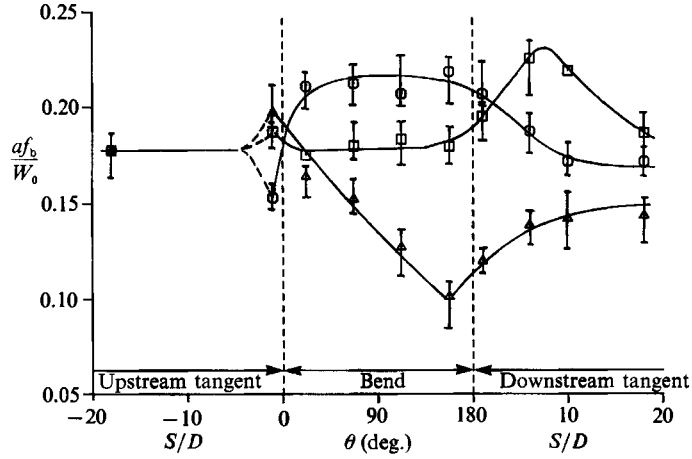

FIGURE 9. Bursting frequency in a pipe bend normalized with outer variables: —△— inner bend, —□— outer bend, —○— top of the bend.

entrance could be attributed to the slight rise in wall shear stress observed at this location (compare figures 7*a* and 9). Since the increased shear stress augments turbulence production in the near-wall region, sublayer bursting at the wall is expected to be increased by this activity. Within the bend, the flow experiences a streamwise convex curvature near the inner bend. Therefore, the resulting stabilizing effect (Clauser & Clauser 1937; So & Mellor 1973) contributes to a reduction of sublayer bursting and this is a major cause of bursting frequency reduction along the inner bend.

Contrary to expectation, the bursting frequency does not show any increase on the outer bend within the bend itself. Furthermore, the bursting frequency starts to increase only as the flow comes out of the bend and enters the downstream straight pipe. Along the outer bend, two effects are dominant – the streamwise concave curvature and the Dean-type secondary flow. So & Mellor (1975) and Moser & Moin (1987) have observed the formation of Taylor–Görtler vortices on a concave surface. Such structures could enhance the formation of counter-rotating vortices within the sublayer and hence bursting. On the other hand, the secondary flow impinges on the outer bend and this tends to suppress bursting there. Since the two effects are not complementary, no net change in bursting is observed along the outer bend. As the

flow comes out of the bend, the centrifugal force disappears abruptly, while the memory of the streamline curvature still remains with the flow. This causes a sudden deceleration of the secondary flow and a relaxation of the jet impingement effect on the flow along the outer bend. Furthermore, the relaxation of the bend curvature also tends to create a second secondary cell near the outer bend (Rowe 1970; Lai *et al.* 1989), and changes the flow behaviour from that of jet impingement to that of boundary-layer merging. It is this destruction of jet impingement that causes the bursting frequency to increase on the outer bend. Beyond $S/D = 6$, the influence of the external effects slowly disappears and the flow starts its long recovery to a fully developed straight pipe condition.

It is not clear why the bursting frequency is reduced on the top of the pipe before the flow enters the bend. However, as the flow enters the bend, a Dean-type secondary motion is superimposed on the axial flow. Even though the magnitude of the secondary motion is not large, it sets up a flow over the circumference of the pipe, the curvature of which is concave. This introduces a destabilizing concave curvature effect on the flow and hence contributes to an increase in bursting frequency. The bursting frequency remains fairly constant within the bend itself, because the strength of the secondary motion remains fairly constant along the bend (Anwer *et al.* 1989). Towards the bend exit, the secondary motion strength begins to decrease and this leads to a concomitant decrease of bursting frequency on the top of the bend.

In the downstream straight pipe, the bursting frequency at the top is the first to return to its fully developed straight pipe value. However, the bursting frequencies at the inner and outer bends are far from those measured in a fully developed straight pipe flow, even at $S/D = 18$. This result is consistent with the velocity and turbulence measurements of Anwer *et al.* (1989) and the total pressure measurements of Rowe (1970) which showed that recovery from bend curvature is still not complete at 29 diameters downstream of the bend exit. Similar results were also observed by Klebanoff & Diehl (1952) in their investigation of the relaxation of an artificially thickened boundary layer. They found that the perturbed boundary layer returned to an undisturbed flow condition in the free stream quickly, but perturbation in the near-wall region persisted for a much longer distance. These results, therefore, point to the fact that viscosity acts slowly to destroy extra turbulence production due to bend curvature or other external effects.

The bursting frequency shown in figure 9 is scaled with the outer variables. Since the present objective is to compare the bursting frequency in the bend section with that in a straight pipe, the scaling with outer variables is justified because they stay constant within the bend, while the inner variables, such as the friction velocity, are changing with axial distance along the bend. Blackwelder & Haritonidis (1983) and Luchik & Tiederman (1987) have argued that bursting frequency should be scaled with the inner variables and not with the outer variables as commonly carried out by other researchers. Hence, the present results are also scaled with the inner variables (friction velocity and kinematic viscosity), and are shown in figure 10. Similar to what has been observed in a boundary layer, the bursting frequencies along all three ψ-locations on the circumference in the straight pipe and the curved bend tend to collapse on a single curve. The exception is the bursting frequency at the outer bend of the curved section. This implies that some kind of local similarity exists at $\psi = 0°$ and 90° locations even under the influence of bend curvature. It also shows that the contribution of bursting towards the generation of turbulence stays about the same around the circumference of the pipe, with the exception of the outer bend.

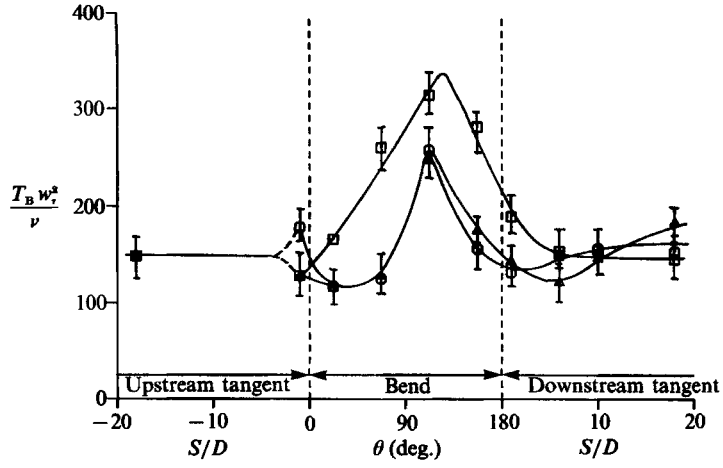

FIGURE 10. Bursting frequency in a pipe bend normalized with inner variables: —△— inner bend, —□— outer bend, —○— top of the bend.

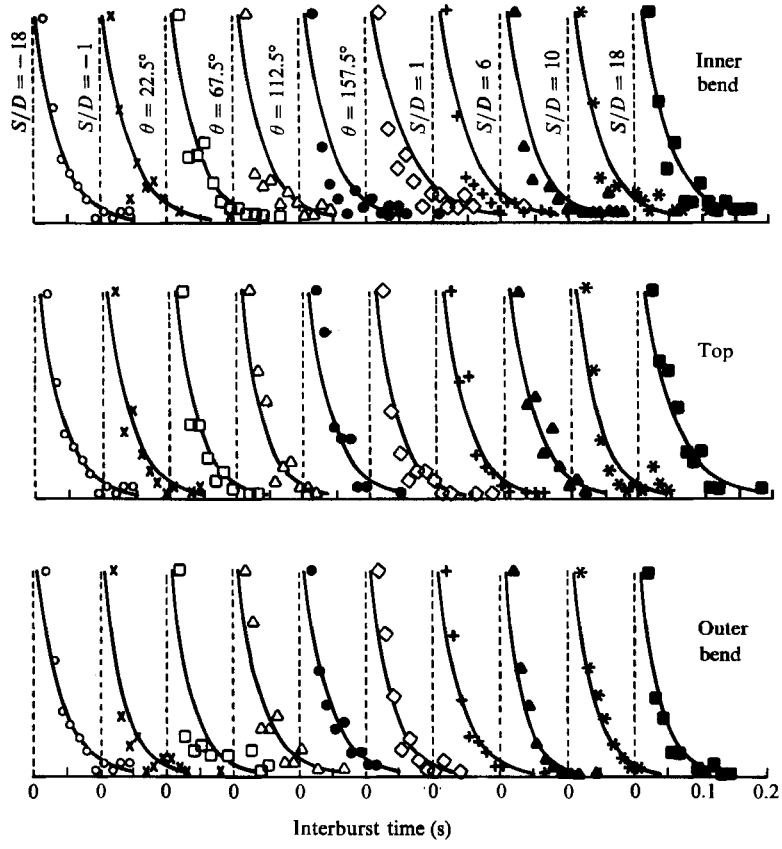

FIGURE 11. Interburst time distribution.

A strong similarity can be observed between the behaviour of the bursting frequency and the r.m.s. values, $(\overline{\tau_w'^2})^{\frac{1}{2}}$ (N/m^2), of the wall shear stress (compare figures 7 and 9). Along the outer bend, the r.m.s. value stays fairly constant within the bend, but increases as the flow exits the bend. This similarity is essentially a direct consequence of the VITA technique. Since the VITA technique calculates a 'local variance' of the signal and detects a burst if the local variance is higher than a prescribed value, a direct correlation between the bursting frequency and the variance of the signal is expected. In general, an overall qualitative agreement is observed between the behaviour of the bursting frequency and the r.m.s. value of the wall shear stress for all locations at the inner bend and at the top of the bend.

The skewness, $\overline{\tau_w'^3}/(\overline{\tau_w'^2})^{\frac{3}{2}}$, and the kurtosis, $\overline{\tau_w'^4}/(\overline{\tau_w'^2})^2$, of the wall shear stress are also shown in figure 7. These results show that the skewness and the kurtosis are increased on the inner bend. However, they are least affected on the top of the bend and on the outer bend.

4.3. *Interburst time distribution*

Bogard & Tiederman (1986) have shown that the times between two consecutive bursts have an exponential distribution. This means that not only is the bursting rate random in time, but also that the bursts are independent of each other. Interburst time distributions were calculated in the present analysis and are shown in figure 11. In order to check for the exponential behaviour, a least-square exponential fit was also calculated using all the actual data points and are plotted as solid curves in figure 11. For a fully developed pipe flow, the curve represents the measured interburst time distribution very well. This means that bursts are random in time and independent of each other in the straight pipe in this study. As the flow enters the bend, the exponential curve starts to deviate from the actual data obtained along the inner bend. In the downstream straight pipe, the exponential nature of the interburst time distribution is again evident. The perturbation of the exponential behaviour is most severe on the inner bend. This means that at certain locations along the inner bend, bursts either lose their randomness in time, or are no longer independent of each other. It is also observed that the exponential curve fits the data very well on the top of the bend and along the outer bend. This means that even with increased mean shear and variance, the bursting process retains its randomness and independence.

4.4. *Spectral content and histogram*

Plots of the energy spectra, $E_\tau(f)$, of the wall shear stress versus the frequency, f, are shown in figure 12 (a–c). In these plots the $-\frac{5}{3}$ slope is also shown to indicate the extent of the inertial subrange. The effect of the bend curvature on the spectra is quite evident. Along the inner bend the shear stress decreases gradually with increasing θ. This results in a gradual reduction of the strain rate of the near-wall flow. The resultant lower strain rate reduces the stretching of the eddies. Consequently, the energy cascading process is perturbed, and large eddies do not transfer their energy to the small eddies at the same rate as that observed in the straight pipe. This effect on energy transfer continues until the flow reaches around $\theta = 157.5°$. At this point, the flow begins to readjust itself as the bend exit is approached. The readjustment continues beyond $S/D = 18$ because the wall shear spectrum at this location still differs from that at $S/D = -18$. This observation is consistent with that of Klebanoff & Diehl (1952) who studied an artificially perturbed boundary layer. It should be pointed out that both the inertial subrange and the equilibrium range of the spectra are affected by bend curvature along the

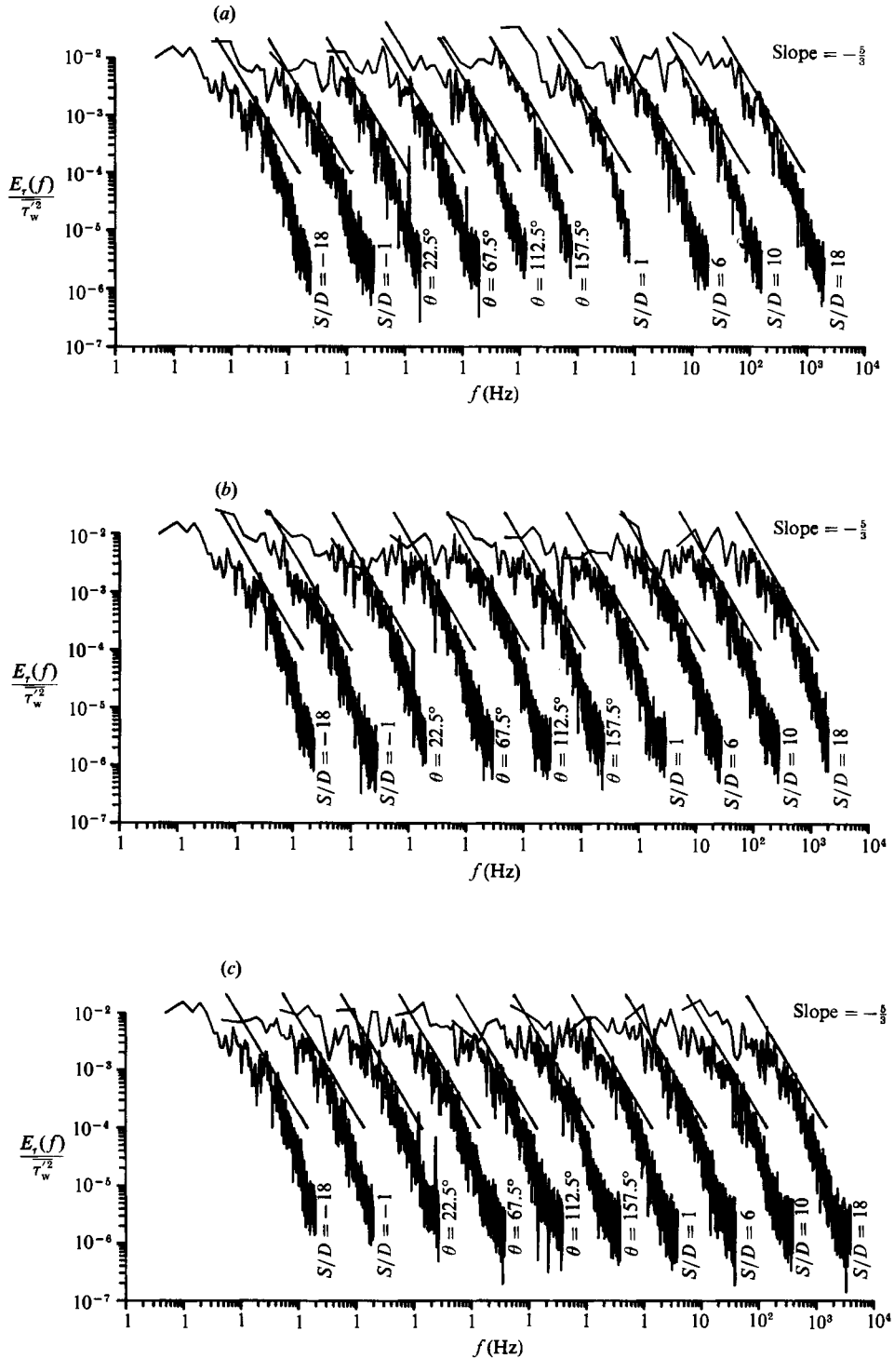

FIGURE 12. Spectral content of wall shear stress signal along (*a*) the inner bend, (*b*) the outer bend, (*c*) the top of the bend.

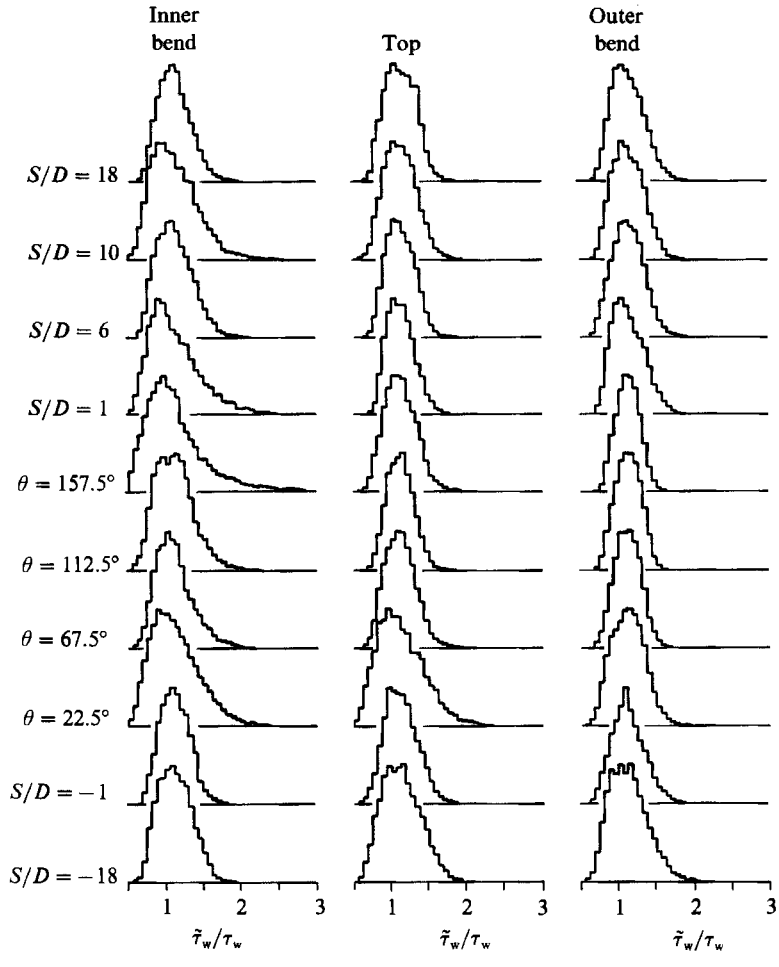

FIGURE 13. Histograms of wall shear stress signal.

inner bend. Again, their recovery to the unperturbed condition is slow and consistent with other results discussed above. Along the outer bend, the strain rate is higher because of the higher wall shear stress. Consequently, the inertial subrange and the equilibrium range in the wall shear spectra are observed to increase slightly, but the increase is not as prominent as the decrease shown on the inner bend. Finally, the spectral content of the wall shear is not affected by bend curvature along the top of the bend.

The histograms of the shear stress signals are shown in figure 13. For a fully developed straight pipe flow, the histogram is close to a normal distribution. The perturbation of wall shear by bend curvature is clearly illustrated by the histograms, especially along the inner bend, where a gradual deviation from the normal distribution is observed. Unlike the spectral content of the wall shear, the histogram asymptotes to its undisturbed distribution on the inner bend, the outer bend, and the top of the bend at $S/D = 18$. This agrees well with the behaviour of the skewness and the kurtosis shown in figure 7.

5. Conclusions

The following conclusions can be drawn from this study.

(i) The VITA technique can be used to identify bursting events in wall shear stress signals in complex turbulent flows like the one studied here. Since the timescale of the signal is very small, a high sampling rate is required.

(ii) It is evident that external effects play a major role in sublayer bursting. Convex curvature tends to stabilize the flow, hence reduces the bursting frequency. On the other hand, concave curvature enhances the bursting frequency and so does flow deceleration.

(iii) Perturbation of the bursting phenomenon by external effects takes a long time to decay. The perturbed bursting process persists even after the external effects have been relaxed and the wall static pressure recovers. In general, most of the higher-order statistics associated with the wall shear stress remain perturbed for a considerably longer distance than the measured wall static pressure.

(iv) A direct correlation is noticed between the bursting frequency and the variance of the wall shear stress. This is essentially a consequence of the detection algorithm.

(v) A qualitative agreement is observed between the bursting frequency and the spectral content of the wall shear stress.

(vi) Bursting loses its randomness and/or independence at the inner bend. As a result, at some location within the bend the interburst time distribution loses its exponential behaviour.

(vii) The spectral content of the wall shear stress reveals that both the inertial subrange and the equilibrium range are reduced on the inner bend.

Research support by the Office of Naval Research under Grant No. N0014-81-K-0428 is gratefully acknowledged.

REFERENCES

ACHIA, B. U. & THOMPSON, P. W. 1977 Structure of the turbulent boundary layer in drag reducing pipe flow. *J. Fluid Mech.* **81**, 439–464.

ANWER, M., SO, R. M. C. & LAI, Y. G. 1989 Perturbation by and recovery from bend curvature of a fully developed turbulent pipe flow. *Phys. Fluids* A **1**, 1387–1397.

AZZOLA, J., HUMPHEREY, J. A. C., IACOVIDES, I. & LAUNDER, B. E. 1986 Developing turbulent flow in a U-bend of circular cross section. *Trans. ASME* I: *J. Fluids Engng* **108**, 214–220.

BAKEWELL, H. P. & LUMLEY, J. L. 1967 Viscous sub-layer and adjacent wall region in turbulent pipe-flow. *Phys. Fluids* **10**, 1880–1889.

BELLHOUSE, B. J. & SCHULTZ, D. L. 1966 Determination of mean and dynamic skin friction, separation and transition in low-speed flow with a thin-film heated element. *J. Fluid Mech.* **24**, 379–400.

BLACKWELDER, R. F. 1978 The bursting process in turbulent boundary layers. *Workshop on Coherent Structure of Turbulent Boundary Layer*, pp. 211–224. AFOSR/Lehigh University.

BLACKWELDER, R. F. & HARITONIDIS, J. H. 1983 Scaling of the bursting frequency in turbulent boundary layers. *J. Fluid Mech.* **132**, 87–112.

BLACKWELDER, R. F. & KAPLAN, R. E. 1976 On the wall structure of the turbulent boundary layer. *J. Fluid Mech.* **76**, 89–112.

BOGARD, D. G. & TIEDERMAN, W. G. 1986 Burst detection with single-point velocity measurements. *J. Fluid Mech.* **162**, 389–413.

BROWN, G. L. & THOMAS, A. S. W. 1977 Large structure in a turbulent boundary layer. *Phys. Fluids* **20**, S243–S252.

CLAUSER, L. M. & CLAUSER, F. 1937 The effect of curvature on the transition from laminar to turbulent boundary layer. *NACA TN* 613.

COLES, D. 1978 A model for flow in the viscous sub-layer. *Workshop on Coherent Structure of Turbulent Boundary Layers*, pp. 462–475. AFOSR/Lehigh University.

CORINO, E. R. & BRODKEY, R. S. 1969 A visual investigation of wall region in turbulent flow. *J. Fluid Mech.* **37**, 1–30.

CORRSIN, S. 1957 Some current problems of turbulent shear flows. *Proc. 1st. Naval Hyd. Symp.* Nat. Acad. Sci./Nat. Res. Counc. 373.

DURRETT, R. P., STEVENSON, W. H. & THOMPSON, H. D. 1985 Radial and axial turbulent flow measurements with an LDV in an axisymmetric sudden expansion air flow. *Int. Symp. on Laser Anemometry* (ed. A. Dybbs & P. A. Pfund), pp. 127–133. ASME special publ. FED-33.

FALCO, R. E. 1978 Wall layer structure of a turbulent boundary layer. *Bull. Am. Phys. Soc.* II, **23**, 1000.

HEAD, M. R. & BANDYOPADHYAY, P. 1978 Combined flow visualization and hot-wire measurements in turbulent boundary layers. *Workshop on Coherent Structure of Turbulent Boundary Layer*, pp. 98–125. AFOSR/Lehigh University.

HEAD, M. R. & BANDYOPADHYAY, P. 1981 New aspects of turbulent boundary layer structure. *J. Fluid Mech.* **107**, 297–338.

HEIDRICK, T. R., BANERJEE, S. & AZAD, R. S. 1977 Experiments on the structure of turbulence in fully developed pipe flow. Part 2. A statistical procedure of identifying 'bursts' in the wall layer and some characteristics of flow during bursting periods. *J. Fluid Mech.* **56**, 705–723.

JOHANSSON, A. V. & ALFREDSSON, P. H. 1982 On the structure of turbulent channel flow. *J. Fluid Mech.* **122**, 295–314.

KIM, H. T., KLINE, S. J. & REYNOLDS, W. C. 1971 The production of turbulence near a smooth wall in a turbulent boundary layer. *J. Fluid Mech.* **50**, 133–160.

KIM, J. & MOIN, P. 1986 The structure of vorticity in turbulent channel flow. Part 2. Study of ensembled averaged field. *J. Fluid Mech.* **162**, 339–364.

KLEBANOFF, P. S. 1955 Characteristics of turbulence in a boundary layer with zero pressure gradient. *NACA TR* 1247.

KLEBANOFF, P. S. & DIEHL, A. W. 1952 Some features of artificially thickened fully developed turbulent boundary layer with zero pressure gradient. *NACA Rep.* 1110.

KLINE, S. J. 1978 The role of visualization in the study of the structure of the turbulent boundary layer. *Workshop on Coherent Structures of Turbulent Boundary Layers*, pp. 1–27. AFOSR/Lehigh University.

KLINE, S. J., REYNOLDS, W. C., SCHRAUB, F. A. & RUNDSTADLER, P. W. 1967 The structure of turbulent boundary layers. *J. Fluid Mech.* **30**, 741–773.

KOBASHI, Y. & ICHIJO, M. 1986 Wall pressure and its relation to turbulent structure of a boundary layer. *Expts Fluids* **4**, 49–55.

LAI, Y. G., SO, R. M. C., ANWER, M. & HWANG, B. C. 1989 Calculation of curved-pipe flow using a Reynolds-stress closure. *Phys. Fluids* (submitted).

LAUFER, J. 1954 The structure of a turbulence in fully developed pipe flow. *NACA Rep.* 1174.

LIGRANI, P. M. & BRADSHAW, P. 1987 Spatial resolution and measurement of turbulence in viscous sub-layer using sub-miniature hot-wire probes. *Expts Fluids* **5**, 407–417.

LU, S. S. & WILLMARTH, W. W. 1973 Measurements of the structure of Reynolds stress in a turbulent boundary layer. *J. Fluid Mech.* **60**, 481–511.

LUCHIK, T. S. & TIEDERMAN, W. G. 1987 Timescale and structure of ejection and burst in turbulent channel flows. *J. Fluid Mech.* **174**, 529–552.

MAUTNER, T. S. & VAN ATTA, C. W. 1986 Wall shear stress measurements in the plane of symmetry of a turbulent spot. *Expts Fluids* **4**, 153–162.

MENENDEZ, T. S. & RAMAPRIAN, B. R. 1985 The use of flush-mounted hot-film gauges to measure skin friction in unsteady boundary layers. *J. Fluid Mech.* **161**, 139–159.

MOIN, P. & KIM, J. 1985 Analysis of vorticity field in turbulent channel flows. *J. Fluid Mech.* **155**, 441–464.

MOSER, M. D. & MOIN, P. 1987 The effects of curvature in wall bounded turbulent flows. *J. Fluid Mech.* **175**, 479–510.

PERRY, A. E. & CHONG, M. S. 1982 On the mechanism of wall turbulence. *J. Fluid Mech.* **119**, 173–217.

PERRY, A. E., LIM, T. T. & TEH, E. W. 1981 A visual study of turbulent spots. *J. Fluid Mech.* **104**, 387–405.

ROWE, M. 1970 Measurements and computation of flow in pipe bends. *J. Fluid Mech.* **43**, 771–783.

SABOT, J. & COMTE-BELLOT, G. 1976 Intermittency of coherent structures in the core region of fully developed turbulent pipe flow. *J. Fluid Mech.* **74**, 767–796.

SMITH, C. R. 1978 Visualisation of a turbulent boundary layer structure using a moving hydrogen bubble-wire probe. *Workshop on Coherent Structure of Turbulent Boundary Layer*, pp. 48–94. AFOSR/Lehigh University.

SO, R. M. C. & MELLOR, G. L. 1973 Experiment on convex curvature effects in turbulent boundary layer. *J. Fluid Mech.* **60**, 43–62.

SO, R. M. C. & MELLOR, G. L. 1975 Experiments on turbulent boundary layer on a concave wall. *Aero. Quart.* **26**, 25–40.

STRICKLAND, J. H. & SIMPSON, R. L. 1975 'Bursting' frequency obtained from wall shear stress fluctuations in a turbulent boundary layer. *Phys. Fluids* **18**, 306–308.

THEODORSEN, T. 1952 Mechanism of turbulence. *Proc. 2nd Midwester Conf. Fluid Mech.*, p. 1.

THEODORSEN, T. 1955 The structure of turbulence. *50 Jahre Grenzschichtforschung* (ed. H. Görtler & W. Tollmein), p. 55.

UEDA, H. & MIZUSHIMA, T. 1979 Turbulence structure in the inner part of the wall region in a fully developed turbulent tube flow. *Proc. 5th Biennial Symp. on Turbulence*, p. 357.